LETTERS
PUBLISHED ONLINE: 24 JULY 2011 | DOI: 10.1038/NMAT3071

nature materials

Epitaxial growth of three-dimensionally architectured optoelectronic devices

Erik C. Nelson[1], Neville L. Dias[2], Kevin P. Bassett[2], Simon N. Dunham[1], Varun Verma[2], Masao Miyake[3], Pierre Wiltzius[4], John A. Rogers[1], James J. Coleman[2], Xiuling Li[2] and Paul V. Braun[1]★

Optoelectronic devices have long benefited from structuring in multiple dimensions on microscopic length scales. However, preserving crystal epitaxy, a general necessity for good optoelectronic properties, while imparting a complex three-dimensional structure remains a significant challenge. Three-dimensional (3D) photonic crystals are one class of materials where epitaxy of 3D structures would enable new functionalities. Many 3D photonic crystal devices have been proposed, including zero-threshold lasers[1,2], low-loss waveguides[3–5], high-efficiency light-emitting diodes (LEDs) and solar cells[6–8], but have generally not been realized because of material limitations. Exciting concepts in metamaterials, including negative refraction and cloaking, could be made practical using 3D structures that incorporate electrically pumped gain elements to balance the inherent optical loss of such devices[9]. Here we demonstrate the 3D-template-directed epitaxy of group III–V materials, which enables formation of 3D structured optoelectronic devices. We illustrate the power of this technique by fabricating an electrically driven 3D photonic crystal LED.

Despite significant efforts over the past two decades, the development of 3D structured materials that possess the requisite low defect density for optoelectronic functionality has remained elusive. There are many pathways by which to impart a complex 3D structure into amorphous or polycrystalline materials[10–13], however such materials have poor electrical properties. In particular, for optoelectronic devices where long carrier lifetimes are required, it will almost certainly be necessary to form the 3D structure from a single-crystal, direct-bandgap semiconductor to minimize undesired recombination and other losses. Approaches based on the patterning of single-crystal starting materials, including anisotropic dry etching[14], wafer bonding[15] and layer-by-layer[16,17] assembly techniques, are intriguing. However, they are limited to specific 3D structures and materials, and often contain undesirable defects; thus, as far as we are aware, optoelectronic activity has not been demonstrated so far from any device formed using these approaches.

Here we demonstrate the epitaxial growth of group III–V semiconductor 3D nanostructured materials, including those containing light-emitting heterostructures, by selective area epitaxy (SAE) through a 3D template. As traditionally performed, selective area epitaxy is a process during which a two-dimensional (2D), typically oxide, mask is patterned on a semiconductor wafer and material is subsequently grown by metal–organic chemical vapour deposition (MOCVD). Growth occurs only on the exposed regions of semiconductor, resulting in a patterned film. We show that a 3D nanostructured mask can be used in conjunction with MOCVD to epitaxially grow a 3D structured, optoelectronically active, GaAs-based material—in this case, a 3D photonic crystal. Epitaxy is preserved even as the GaAs grows through the complex geometry of the template.

A representative 3D photonic crystal is shown schematically and in the scanning electron microscope (SEM) cross-section image in Fig. 1a. The SEM image shows a colloidal crystal template that has been partially filled from the substrate upwards with GaAs by means of selective area epitaxy. Growth initiates in the [001] direction from the GaAs(001) wafer surface, however to grow around the template the growth front propagates in various directions. This is observed in the inset of Fig. 1a, where the growth front moves off-normal to propagate around the template. After the template is almost completely filled (Fig. 1b), it is etched, leaving a porous 3D semiconductor structure (Fig. 1c). We intentionally underfill the template to prevent formation of a sealed surface, which would lead to difficulty removing the template. Three-dimensional SAE was also performed through polymer templates created using interference lithography by first converting the template to a thermally stable material such as alumina (Fig. 1d), followed by growth of GaAs and removal of the template (Fig. 1e), providing a route to almost any 3D structure, given the versatility of interference lithography[13,18,19].

The fact that the growth begins at the substrate, and proceeds upwards, is only evidence of selective area deposition, not epitaxy. Epitaxy of the photonic crystals was quantitatively confirmed using $2\theta/\omega$ X-ray diffraction (Fig. 2a), electron diffraction (Fig. 2c,d) and texture measurements (Fig. 2b) on samples after template removal (for example Fig. 1c). In the $2\theta/\omega$ measurements only the GaAs(002)/(004)/(006) peaks were detected, indicating a common out-of-plane lattice spacing between the photonic crystal and the substrate. The crystalline nature of the deposit (Fig. 2c) was confirmed by electron diffraction (Fig. 2d). Epitaxy was confirmed by pole figure analysis (Fig. 2c), which shows four strong peaks at 45° originating from (220) reflections. The pole figure also shows several additional peaks that are due to (111) twinning in the film (see Supplementary Table S1), which often occurs during growth of group III–V nanostructures, such as nanowires.

Traditional 2D selective area epitaxy relies on a strong preference for growth on the semiconductor substrate rather than the mask material[20–23]. When applied to planar device fabrication, if a small amount of nucleation occurs on the mask surface the nuclei are typically removed when the mask is etched. However, if nucleation occurs on the surface of our 3D masks (Fig. 3a) a polycrystalline film will result, because the surface nuclei penetrate

[1]Department of Materials Science and Engineering, Beckman Institute, and Frederick Seitz Materials Research Laboratory, Urbana, Illinois 61801, USA, [2]Department of Electrical and Computer Engineering, Urbana, Illinois 61801, USA, [3]Graduate School of Energy Science, Kyoto University, Kyoto 606-8501, Japan, [4]Department of Physics, University of California Santa Barbara, Santa Barbara, California 93106, USA. *e-mail: pbraun@illinois.edu.

© 2011 Macmillan Publishers Limited. All rights reserved.

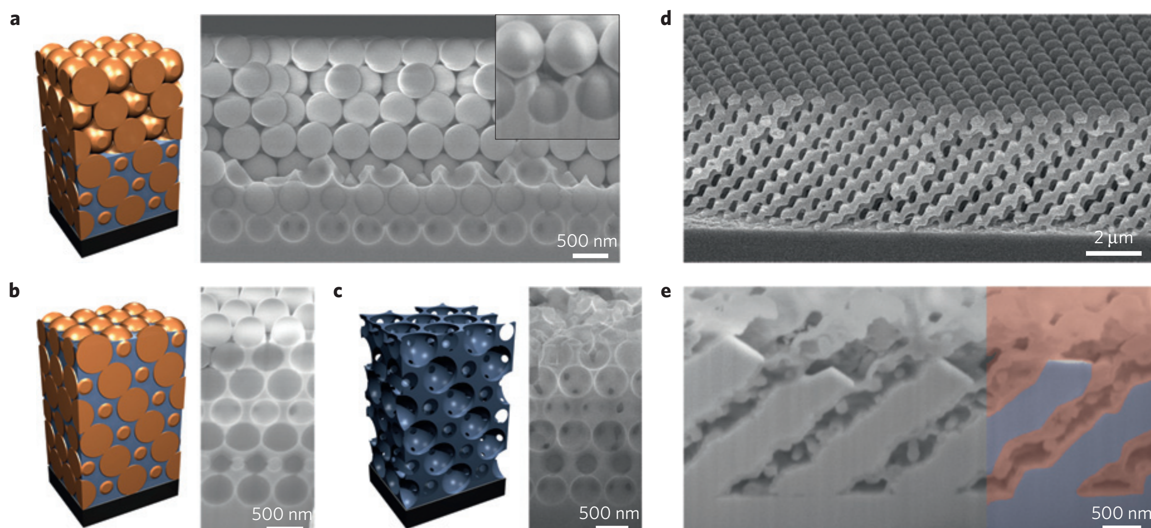

Figure 1 | Three-dimensionally patterned GaAs photonic crystals. a, Schematic and SEM of a 3D photonic crystal template partially filled with GaAs by epitaxy. Inset highlights off-normal growth directions that occur when the GaAs grows around the template. Schematic and focused ion-beam cross-section SEM images of **b**, GaAs filled template and **c**, inverted (template removed) GaAs structure. **d**, Polymer template formed by multibeam interference lithography. The template was filled with alumina and the polymer was removed, providing a template with high temperature stability for GaAs growth. **e**, The GaAs filled the alumina template. GaAs is shown in blue and alumina in red in the colourized image.

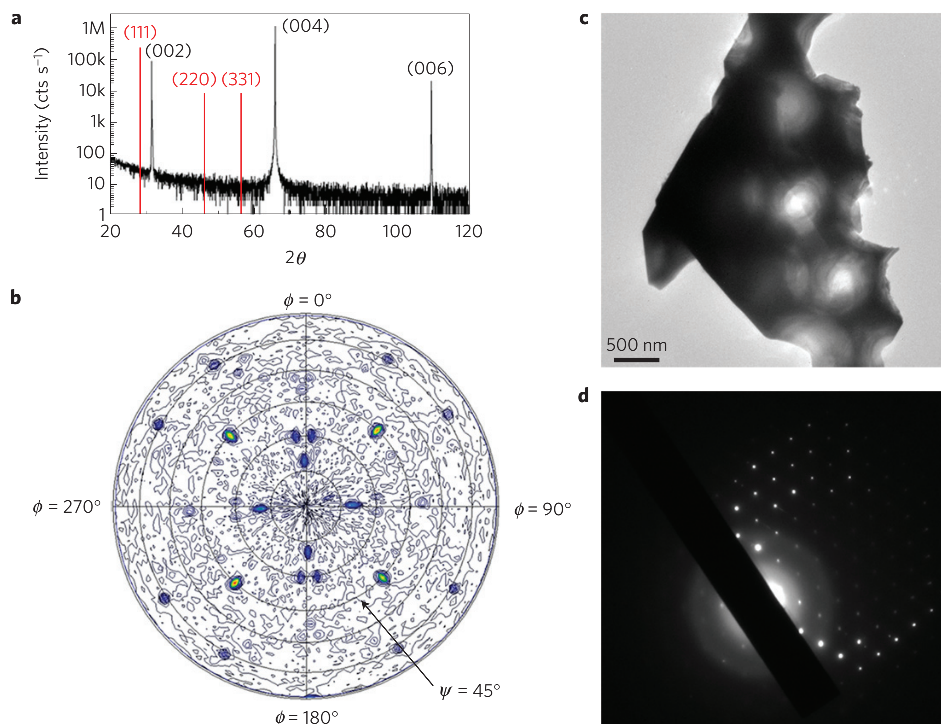

Figure 2 | Verification of epitaxy during 3D patterned growth. a, $2\theta/\omega$ X-ray diffraction measurement of a GaAs 3D photonic crystal. The red lines and labels are the expected locations for polycrystalline reflection peaks, which are not observed. **b**, Pole figure (220) X-ray diffraction measurement of the same photonic crystal. The individual peaks from the (220) family of planes are observed at $\psi = 45°$, rather than a circumferential ring of intensity, as are peaks due to (111) twinning. The scale rings are in 15° increments. **c**, Transmission electron micrograph of a small piece of a GaAs photonic crystal grown by 3D SAE. **d**, Electron diffraction from the structure in **c**.

downward into the template as shown in Fig. 3b and merge with the upward propagating growth front, resulting in incorporation of polycrystalline material into the 3D structure. Elimination of surface nucleation is a critical component for successful 3D SAE. It is known that an interplay between the growth temperature, reactor pressure, and the partial pressures of the group III precursors controls the rate of heterogeneous nucleation during SAE (refs 24,25; see Supplementary Information). Diffusion of the precursors through the 3D template is reduced in comparison with the bulk gas phase, resulting in an increased partial pressure of the source materials over the 3D mask, which affects the heterogeneous nucleation behaviour. Therefore, conditions for selective growth are different for 2D and 3D masks and must be elucidated[25].

© 2011 Macmillan Publishers Limited. All rights reserved.

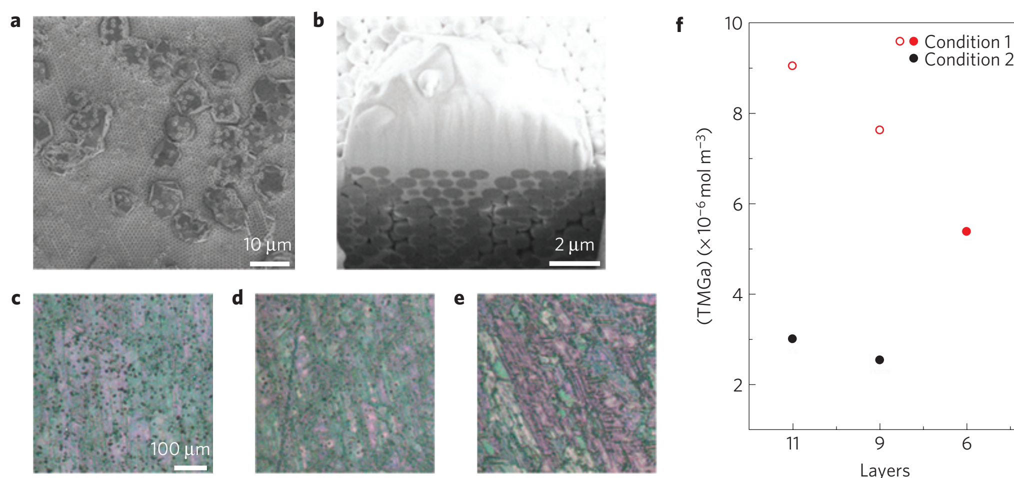

Figure 3 | Heterogeneous nucleation behaviour during 3D selective area epitaxy. a, Top surface of a 3D template after growth of GaAs under conditions that yield polycrystalline nucleation on the mask. **b**, Focused ion-beam cross-section through a polycrystalline nuclei. **c–e**, Optical micrographs of 3D template surface from regions of 11, 9 and 6 layers, respectively, with varying degrees of polycrystalline nucleation (black spots). **f**, Plot of partial pressure of monomethyl gallium over the 3D mask surface as a function of template thickness (number of layers), calculated by finite-element modelling. Red circles are under the conditions used to grow the samples shown in **c–e** and black circles are after a reduction of the inlet flow rate of the group III source, as described in the text. Open circles denote conditions where nucleation occurs and closed circles denote nucleation-free growth.

The rate of heterogeneous nucleation is also strongly influenced by the thickness of the template (for example the number of layers or periods) because this affects the partial pressure of precursor over the template owing to the reduced diffusivity through the 3D structure. The effect of template thickness or diffusion distance on precursor partial pressure is presented in Fig. 3c–e, where the nucleation density is high, moderate and approaching zero as the number of layers of the template decreases from 11 to 9 to 6. Finite element modelling of the group III source concentration profile over the 3D mask was used to calculate the partial pressure threshold for heterogeneous nucleation[22,25]. Diffusion through the 3D mask was modelled using Knudsen and Enskog diffusion[26], allowing calculation of the partial pressure above the mask for the structures with 11, 9 and 6 layers (Fig. 3f, red circles). The threshold partial pressure for nucleation on the surface of this template is defined to be approximately the partial pressure over the six-layer mask (Fig. 3e), as nucleation did not occur in this region. The reactor pressure and inlet precursor pressures are chosen such that the calculated group III partial pressure over even the thickest region is maintained well below the nucleation threshold (Fig. 3f, black circles), resulting in nucleation-free growth (for example Fig. 1a).

Epitaxial growth alone is not sufficient for optoelectronic device operation. Surface recombination is a significant concern in group III–V optoelectronic devices, and the porous material shown in Fig. 1c has a large surface area. Unoccupied bonds at surfaces act as carrier traps, resulting in non-radiative recombination and significant decreases in device efficiency. This can be prevented by growth of a wider bandgap semiconductor passivation layer on exposed surfaces, creating a potential barrier that prevents carriers from reaching unoccupied bonds. We demonstrate that this may be achieved on a non-planar, 3D material architecture by growing a GaAs/AlGaAs/GaAs heterostructure on all exposed surfaces of the 3D structure after removal of the template (Fig. 4c, a monolayer to highlight the faceting; multilayer structures are shown in Supplementary Fig. S3b,c). The approximately 10 nm $Al_{0.75}Ga_{0.25}As$ layer has a larger electronic bandgap than InGaAs or GaAs, creating an effective potential barrier for carriers in the structure, whereas the outermost GaAs layer serves to prevent oxidation of the AlGaAs. GaAs growth through the template is defined by the template geometry; however, after removal of the template, the AlGaAs growth will occur at different rates for different crystallographic directions.

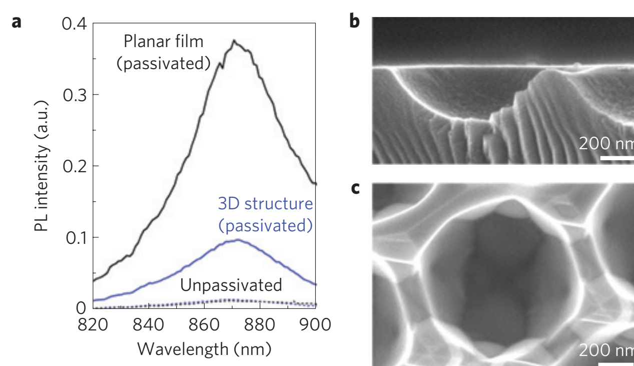

Figure 4 | Surface passivation of 3D structured group III–V materials. a, Photoluminescence measurements of a 3D structured (blue) and unpatterned (black) material before (dashed) and after (solid) passivation. Before passivation, the photoluminescence of both samples is low and essentially overlaps. **b**, GaAs structure after inversion grown partially through the first layer of a template. The curvature imparted by the template is clearly visible. **c**, The structure from **b** after growth of a passivation layer (GaAs/AlGaAs/GaAs). The epitaxial nature of the passivation layer is highlighted by the faceting of the structure.

The smooth curvature of the template (Fig. 3b) thus gives way to the faceted structure seen in Fig. 3c, as certain planes grow faster than others, indicating epitaxial growth of the passivation layer on the underlying structure. The effectiveness of the passivation process is characterized by the intensity of the photoluminescence signal before and after passivation, which is related to the relative amount of surface recombination. Photoluminescence (PL) from a multilayer 3D structure (Supplementary Fig. S3b,c) and planar, unpatterned film grown concurrently on the same substrate exhibit similar PL before passivation and an increase in PL intensity of about an order of magnitude or more after (Fig. 4a). The unpatterned material exhibits approximately three times greater PL signal than the 3D structure after passivation, which is probably due to the greater surface area of the 3D structure (by approximate factor of π). By optimization of the passivation process, 3D structures that exhibit a 20 times increase in photoluminescence after passivation have been obtained (Supplementary Fig. S3a).

© 2011 Macmillan Publishers Limited. All rights reserved.

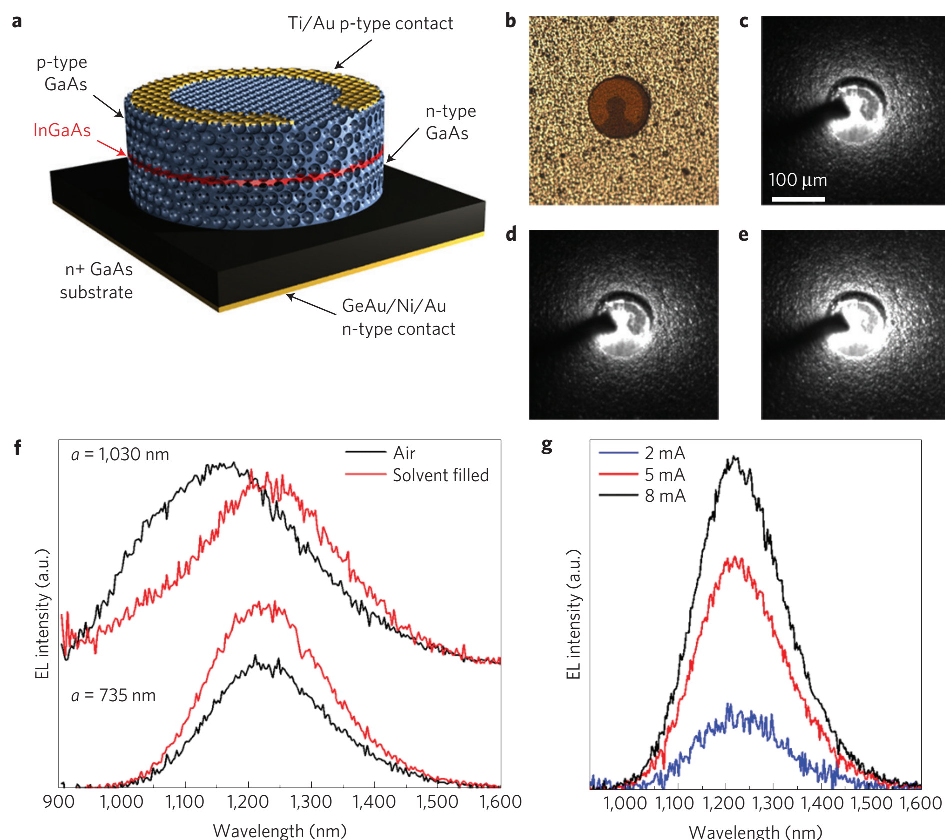

Figure 5 | Electrically driven emission from 3D photonic crystal LED. a, Schematic of a GaAs 3D photonic crystal (blue) containing an InGaAs light-emitting layer (red). The structure is lithographically patterned into the form of a cylindrical mesa with a ring electrode on the top surface (gold). **b**, An optical micrograph of a device under white light illumination showing the Ti/Au ring electrode and the mesa surrounded by the etched GaAs. **c**–**e**, Following current injection (**c**, 2 mA, **d**, 4 mA, **e**, 6 mA) light is emitted and collected by an infrared camera. The light output increases with current. **f**, Electroluminescence (EL) spectra from 3D photonic crystal (PhC) LEDs with lattice constants of 735 nm and 1,030 nm respectively. The shape of the EL spectrum from the 735 nm lattice constant structure does not change when the pores are filled with dodecane, whereas the EL spectrum from the 1,030 nm lattice constant structure changes significantly when the pores are filled with o-xylene. The EL spectra from the 1,030 nm lattice constant structure are shifted up for clarity. **g**, EL spectra from a 3D PhC LED where the emission is not modified by the 3D structure ($a = 735$ nm). The EL intensity increases linearly with current.

The most important feature of the 3D SAE process is that growth begins at the substrate and extends upwards while preserving epitaxy, enabling formation of chemically and electrically complex heterostructures. The complex 3D photonic crystal optoelectronic devices proposed for many years, but never realized, require epitaxially grown 3D structured semiconductor materials with electronic dopants and embedded light-emitting (or collecting) heterojunctions. We demonstrate such a device by fabricating a 3D photonic crystal LED using 3D selective area epitaxy. The device was grown by incorporating an InGaAs layer between lower (Si-doped) and upper (C-doped) GaAs cladding layers during growth through the 3D template, thereby defining a light-emitting heterostructure within a 3D PhC (Fig. 5a). The final 3D photonic crystal LED (Fig. 5a,b) consists of a 120 μm diameter ring electrode on the top of a 3D PhC cylindrical mesa (the mesa serves to prevent current spreading beyond the device boundary). The light-emitting layer consists of approximately 15 nm InGaAs (∼50% indium), bounded on each side by 800 nm of undoped GaAs and thicker layers of Si and C-doped GaAs. An array of devices (Supplementary Fig. S1) show excellent electrical rectification and device-to-device reproducibility. The electrically driven emission from a device is shown in Fig. 5c–e at increasing drive currents. At 2 mA the mesa is emitting light from the entire device, with the strongest emission from the centre of the ring electrode. At higher drive currents the light output increases as expected. Electroluminescence (EL) spectra collected from a device at varying drive currents (Fig. 5g) exhibited a peak emission wavelength of 1,230 nm, which was invariant with drive current. The light output increased linearly over the studied current range (Supplementary Fig. S2).

The emission of two devices with different lattice constants was compared to observe the effects of the PhC structure on the behaviour of the device. The EL spectra were measured before and after infiltration of a solvent (either dodecane or o-Xylene), which is used to change the refractive index contrast of the system. The device with lattice constant $a = 735$ nm shows no change in spectral shape due to infiltration of the solvent, indicating that the interaction of light with the periodic material is minimal. The only change is an increase in the emission intensity due to reduced scatter from the PhC surface when the refractive index contrast is reduced. Conversely, the device with the larger lattice constant ($a = 1{,}030$ nm) demonstrates a noticeable change in peak shape on infiltration of the solvent. This indicates that the emission spectrum of this device is probably modulated by interaction of the InGaAs with the modified optical density of states of the 3D structure. Our band structure calculations suggest this is the case (Supplementary Fig. S4), however we do not draw extensive conclusions, if for no other reason than the fact that the finite thickness of the device leads to a disparity between experiment and band structure calculations.

We have developed a novel 3D SAE approach to create opto-electronically active 3D nanostructured group III–V semiconductor

© 2011 Macmillan Publishers Limited. All rights reserved.

devices. We highlight this approach as a unique route to 3D nanostructured optoelectronic devices by fabricating, and demonstrating electrically driven emission from, a 3D photonic crystal LED, which has not been achieved by other means. The improvements in device performance that will lead to the future application of 3D architectured materials in practical injection electroluminescent devices will require significant efforts to concurrently maximize both optical and electronic properties. Research will need to address, for example, the photonic band structure, electrical conductivity and surface passivation. The end result will be a powerful new optoelectronic device technology with wide applicability.

Methods

Template fabrication. Colloids were synthesized using the methods of Stöber *et al.*[27] and colloidal crystal templates were formed using methods similar to previously published techniques[28]. Sphere diameters used in this work were 520, 760 and 920 nm, which were calcined for 13 h at 720 °C (520 and 760 nm) and 72 h at 600 °C (920 nm). Templates formed using multibeam interference lithography were fabricated in SU-8 photoresist (MicroChem, SU-8 2000 series) using a 532 nm frequency-doubled Nd:YVO_4 laser according to previously published procedures[29,30]. The SU-8 was spin-coated on GaAs substrates that had an e-beam evaporated TiO_2 antireflection coating. Photoresist templates were converted to aluminium oxide using a Cambridge Nanotech ALD system. The photoresist and TiO_2 were removed using a high-pressure (500 mtorr) reactive ion etch (20 s.c.c.m. O_2, 2 s.c.c.m. CF_4) at 150 W (the TiO_2 underneath the alumina was not undercut, allowing the alumina template to remain on the TiO_2-coated GaAs substrate). Silica template removal was achieved using a buffered oxide etch (Transene, Buffered-HF Improved). Alumina templates were removed using a mixture of 10% HF, 45% water and 45% ethanol.

MOCVD growth and device fabrication. MOCVD growth was performed in an Aixtron 200/4 low-pressure MOCVD reactor at 50 mBar. Arsine was used as the group V source and trimethyl gallium, trimethyl indium and trimethyl aluminium were used as group III sources. Growth temperatures ranged from 625 to 800 °C depending on alloy composition and dopant gas used. Samples were doped using disilane (silicon, n type) and carbon tetrabromide (carbon, p type). All substrates were epi-ready GaAs from AXT Technologies (GaAs:Si, $1–3 \times 10^{18}\ cm^{-3}$). Typical precursor flow rates were 15,000 s.c.c.m. H_2, $5 \times 10^{-4}\ mol\ m^{-1}$ arsine, $10^{-5}\ mol\ m^{-1}$ trimethylgallium and $10^{-6}\ mol\ m^{-1}$ trimethylindium. The growth rate varies significantly with PhC lattice constant, fill factor and number of layers. The range of growth rates used for this work was 0.04–0.5 nm s^{-1}. Contacts were evaporated onto the samples using a CHA SEC-600 e-beam/thermal evaporator. The contact materials are Ge/Au/Ni/Au for n-type contacts and Ti/Pt/Au for p-type contacts (n-type contacts were alloyed at 350 °C for 120 s under hydrogen).

Before MOCVD growth, samples were degreased using a 5 m acetone rinse (twice), 2 m methanol rinse, 2 m isopropyl alcohol rinse and then blown dry. Samples were then cleaned in an O_2 plasma (TI Planar Plasma etch) at 300 W for 10 m. Before loading into the reactor an oxide etch was performed using 50:50 HCl: H_2O. Each growth step, apart from AlGaAs capping, was preceded with a 10 m oxide bakeout at 750 °C. For AlGaAs passivation growth processes a 1:10 ammonia:water oxide etch was performed in a glovebox connected to the MOCVD reactor to prevent oxidation of the sample before loading into the reactor; no oxide bakeout was performed.

Devices were fabricated by first depositing n-type contacts on the back surface of each sample and annealing. The ring contact was deposited using a custom-made kapton shadow mask. The samples were then coated with 900 nm of SiO_2 using plasma-enhanced chemical vapour deposition (PECVD) and coated with photoresist (AZ4620). The photoresist was patterned to leave a circle over the ring electrodes and the exposed SiO_2 was subsequently etched using reactive-ion etching (RIE; CF_4, O_2). Samples were dipped in buffered HF (Transene, Buffered HF Improved) for 30 s, rinsed in isopropyl alcohol and dried under nitrogen. A 60 s O_2 plasma clean of the samples was performed, followed by inductively coupled plasma-RIE (ICP-RIE) etching of the GaAs ($SiCl_4$, Ar) to form a mesa. The remaining SiO_2 was then removed with a 5 m dip in buffered HF.

Device characterization. Scanning electron micrographs were taken on a Hitachi S-4800 SEM or FEI Dual Beam 235 focused ion-beam lithography system. X-ray diffraction measurements were performed on a Phillips X'Pert MRD system with a 4-bounce germanium monochromator and PIXcel line detector. Photoluminescence measurements were taken using an Ar-ion laser operating at 488 nm and either an InGaAs detector with a lock-in amplifier or Princeton Instruments Si CCD detector. Electroluminescent samples were measured using a Control Development fibre-coupled InGaAs CCD detector with single-stage thermoelectric cooling. Infrared micrographs were taken using a XenICs Xeva-FPA-1.7-320 attached to a Bruker Hyperion microscope with a 10× glass objective (NA = 0.1).

Received 6 April 2011; accepted 13 June 2011; published online 24 July 2011

References

1. John, S. Strong localization of photons in certain disordered dielectric superlattices. *Phys. Rev. Lett.* **58,** 2486–2489 (1987).
2. Yablonovitch, E. Inhibited spontaneous emission in solid-state physics and electronics. *Phys. Rev. Lett.* **58,** 2059–2062 (1987).
3. Lousse, V. & Fan, S. Waveguides in inverted opal photonic crystals. *Opt. Express* **14,** 868–878 (2006).
4. Johnson, S. G., Villeneuve, P. R., Shanhui, F. & Joannopoulos, J. D. Linear waveguides in photonic-crystal slabs. *Phys. Rev. B* **62,** 8212–8222 (2000).
5. Mekis, A. *et al.* High transmission through sharp bends in photonic crystal waveguides. *Phys. Rev. Lett.* **77,** 3787–3790 (1996).
6. Dong-Ho, K. *et al.* Enhanced light extraction from GaN-based light-emitting diodes with holographically generated two-dimensional photonic crystal patterns. *Appl. Phys. Lett.* **87,** 203508 (2005).
7. Yu, Z., Raman, A. & Fan, S. Fundamental limit of nanophotonic light trapping in solar cells. *Proc. Natl Acad. Sci. USA* **107,** 17491–17496 (2010).
8. Green, M. A. Prospects for photovoltaic efficiency enhancement using low-dimensional structures. *Nanotechnology* **11,** 401–405 (2000).
9. Zheludev, N. I. The road ahead for metamaterials. *Science* **328,** 582–583 (2010).
10. Blanco, A. *et al.* Large-scale synthesis of a silicon photonic crystal with a complete three-dimensional bandgap near 1.5 micrometres. *Nature* **405,** 437–440 (2000).
11. Braun, P. V. & Wiltzius, P. Electrochemically grown photonic crystals. *Nature* **402,** 603–604 (1999).
12. Graugnard, E., Chawla, V., Lorang, D. & Summers, C. J. High filling fraction gallium phosphide inverse opals by atomic layer deposition. *Appl. Phys. Lett.* **89,** 211102 (2006).
13. Shir, D. *et al.* Three dimensional silicon photonic crystals fabricated by two photon phase mask lithography. *Appl. Phys. Lett.* **94,** 011101 (2009).
14. Takahashi, S. *et al.* Direct creation of three-dimensional photonic crystals by a top-down approach. *Nature Mater.* **8,** 721–725 (2009).
15. Noda, S., Tomoda, K., Yamamoto, N. & Chutinan, A. Full three-dimensional photonic bandgap crystals at near-infrared wavelengths. *Science* **289,** 604–606 (2000).
16. Aoki, K. *et al.* Microassembly of semiconductor three-dimensional photonic crystals. *Nature Mater.* **2,** 117–121 (2003).
17. Subramania, G. *et al.* Emission modification of CdSe quantum dots by titanium dioxide visible logpile photonic crystal. *Appl. Phys. Lett.* **95,** 151101 (2009).
18. Campbell, M., Sharp, D. N., Harrison, M. T., Denning, R. G. & Turberfield, A. J. Fabrication of photonic crystals for the visible spectrum by holographic lithography. *Nature* **404,** 53–56 (2000).
19. Jeon, S. *et al.* Three-dimensional nanofabrication with rubber stamps and conformable photomasks. *Adv. Mater.* **16,** 1369–1373 (2004).
20. Azoulay, R., Bouadma, N., Bouley, J. C. & Dugrand, L. Selective MOCVD epitaxy for optoelectronic devices. *J. Cryst. Growth* **55,** 229–234 (1981).
21. Heinecke, H. *et al.* Selective growth of GaAs in the MOMBE and MOCVD systems. *J. Cryst. Growth* **77,** 303–309 (1986).
22. Oh, H-J., Sugiyama, M., Nakano, Y. & Shimogaki, Y. Surface reaction kinetics in metalorganic vapor phase epitaxy of GaAs through analyses of growth rate profile in wide-gap selective-area growth. *Jpn J. Appl. Phys. 1* **42,** 6284–6291 (2003).
23. Scholz, F. *et al.* Selective-area epitaxy of GaInAs using conventional and novel group-III precursors. *J. Cryst. Growth* **145,** 242–248 (1994).
24. Stringfellow, G. B. *Organometallic Vapor-Phase Epitaxy: Theory and Practice* 2nd edn (Academic Press, 1999).
25. Sugiyama, M., Oh, H-J., Nakano, Y. & Shimogaki, Y. Polycrystals growth on dielectric masks during InP/GaAs selective MOVPE. *J. Cryst. Growth* **261,** 411–418 (2004).
26. Poling, B. E., Prausnitz, J. M. & O'Connell, J. P. *Properties of Gases and Liquids* 5th edn (McGraw-Hill, 2000).
27. Stöber, W., Fink, A. & Bohn, E. Controlled growth of monodiperse silica spheres in micron size range. *J. Colloid Interface Sci.* **26,** 62–69 (1968).
28. Jiang, P., Bertone, J. F., Hwang, K. S. & Colvin, V. L. Single-crystal colloidal multilayers of controlled thickness. *Chem. Mater.* **11,** 2132–2140 (1999).
29. Ramanan, V., Nelson, E., Brzezinski, A., Braun, P. V. & Wiltzius, P. Three dimensional silicon-air photonic crystals with controlled defects using interference lithography. *Appl. Phys. Lett.* **92,** 173304 (2008).
30. Chen, Y. C., Geddes, J. B., Lee, J. T., Braun, P. V. & Wiltzius, P. Holographically fabricated photonic crystals with large reflectance. *Appl. Phys. Lett.* **91,** 241103 (2007).

Acknowledgements

We would like to thank M. Sardella and J. Soares of the Materials Research Lab for experimental assistance and helpful discussions. The 3D epitaxy growth process development was supported by the US Army Research Office Award

© 2011 Macmillan Publishers Limited. All rights reserved.

#DAAD19-03-1-0227, fabrication and testing of optoelectronic devices was supported by the US Department of Energy 'Light–Material Interactions in Energy Conversion' Energy Frontier Research Center Award #DE-SC0001293, design of optoelectronic devices was supported by the US Department of Energy 'Center for Energy Nanoscience' Energy Frontier Research Center Award #DE-SC0001013, and optimization of the MOCVD reactor was supported by NSF Award #0749028. E.C.N. would like to thank the Beckman Institute for a Doctoral Fellowship.

Author contributions

E.C.N., V.V., N.L.D., P.V.B. and J.J.C. conceived the initial approach. E.C.N., V.V., N.L.D. and K.P.B. performed the MOCVD growth and evaluated MOCVD data along with J.J.C. and X.L.; remaining data was evaluated by all authors. M.M. and P.W. fabricated the polymeric templates by means of interference lithography and performed conversion to alumina. S.N.D. and E.C.N. developed the device processing; E.C.N. fabricated all devices (with N.L.D. and S.N.D. contributing) and performed all sample characterization and finite element modelling. E.C.N. and P.V.B. wrote the paper.

Additional information

The authors declare no competing financial interests. Supplementary information accompanies this paper on www.nature.com/naturematerials. Reprints and permissions information is available online at http://www.nature.com/reprints. Correspondence and requests for materials should be addressed to P.B.V.

© 2011 Macmillan Publishers Limited. All rights reserved.